Acta Geophysica (2020) 68:723–735
https://doi.org/10.1007/s11600-020-00441-0

RESEARCH ARTICLE - ANTHROPOGENIC HAZARD

Using ground motion prediction equations to monitor variations in quality factor due to induced seismicity: a feasibility study

Vincenzo Convertito[1] · Raffaella De Matteis[2] · Roberta Esposito[3] · Paolo Capuano[3]

Received: 21 January 2020 / Accepted: 3 May 2020 / Published online: 17 May 2020

Abstract

Sub-surface operations for energy production such as gas storage, fluid reinjection or hydraulic fracking may modify the physical properties of the rocks, in particular the seismic velocity and the anelastic attenuation. The aim of the present study is to investigate, through a synthetic test, the possibility of using empirical ground-motion prediction equations (GMPEs) to observe the variations in the reservoir. In the synthetic test, we reproduce the expected seismic activity (in terms of rate, focal mechanisms, stress drop and the *b* value of the Gutenberg-Richter) and the variation of medium properties in terms of the quality factor *Q* induced by a fluid injection experiment. In practice, peak-ground velocity data of the simulated earthquakes during the field operations are used to update the coefficients of a reference GMPE in order to test whether the coefficients are able to capture the medium properties variation. The results of the test show that the coefficients of the GMPE vary during the simulated field operations revealing their sensitivity to the variation of the anelastic attenuation. The proposed approach is suggested as a promising tool that, if confirmed by real data analysis, could be used for monitoring and interpreting induced seismicity in addition to more conventional techniques.

Keywords Induced seismicity · Anelastic attenuation · Ground motion predictive equations

Introduction

The increasing demand of energy is pushing exploration of new sources involving the exploitation of sub-surface resources. In highly populated regions, it is of primary importance that underground industrial operations are made in the safest way to minimize seismic hazard and avoid public concern (e.g., Giardini 2009; Convertito et al. 2012; Grigoli et al. 2017; López-Comino et al. 2018).

It is thus worthwhile that seismicity and medium properties variation induced by field operations have to be monitored. Indeed, it is known from the physics of the rocks that the presence of fluids, in particular when injected at high pressure, in addition to enhance the probability of earthquake occurrence (e.g., due to a reduction in fault strength see Guha 2000), can also modify rock properties and in particular seismic velocity and anelastic attenuation. This is confirmed by both laboratory measurements and data analysis recorded during field operations. For example, Toksoz et al. (1979) and Johnston et al. (1979) conclude that, for sandstone samples, *Q* can change from 100 to 10 based on the saturation and differential pressure. Similar results have been obtained by Hutching et al. (2019) by analyzing earthquakes recorded during field operations at The Geysers geothermal field and by Wcisło et al. (2017) who found high attenuation values ($Q_P \sim 48$ and $Q_P/Q_S < 1$) analyzing seismicity induced by the injection of wastewater in the Costa Molina 2 well in southern Italy. Wandycz et al. (2019) measured the variation of the anelastic attenuation based on the microseismicity recordings in Northern Poland

✉ Vincenzo Convertito
vincenzo.convertito@ingv.it

Raffaella De Matteis
raffaella.dematteis@unisannio.it

Roberta Esposito
resposito@unisa.it; roberta.esposito@ingv.it

Paolo Capuano
pcapuano@unisa.it

[1] Istituto Nazionale di Geofisica e Vulcanologia, Via Diocleziano 328, 80124 Naples, Osservatorio Vesuviano, Italy

[2] Dipartimento di Scienze e Tecnologie, Università Degli Studi del Sannio, Via dei Mulini, 82100 Benevento, Italy

[3] Dipartimento di Fisica "E. R. Caianiello", Università di Salerno, 84084 Fisciano, SA, Italy

during hydraulic stimulation of the two unconventional gas reservoirs. They found that anelastic attenuation varies from 60 to 90 for the Lubocino dataset and has average values of 100 and 124, for P- and S-wave, respectively, in the case of Wysin.

As for the medium properties, the monitoring is currently done using approaches such as 4D seismic velocity, anelastic attenuation or seismic noise tomography (e.g., Calò and Dorbath 2013; Gritto and Jarper 2014; Zang et al. 2014), which require both onerous data processing and are time-consuming.

In the present study, we develop a new technique that could be used together with the previous ones to observe variations in the medium properties. Specifically, we test the sensitivity of the ground-motion prediction equations (GMPEs), which are generally used to estimate ground motion at a specific site or ground-shaking maps (e.g., Convertito et al. 2010), to the variations of the propagation medium properties and, in particular, those related to seismic velocity and anelastic attenuation during subsoil exploitation procedures.

Indeed, GMPEs are equations that correlate a strong ground motion parameter (response variable), such as peak-ground motion acceleration (PGA), peak-ground motion velocity (PGV) or spectral ordinates (Sa) at different structural periods, to predictor variables, such as magnitude and source-to-site distance, through coefficients that must be inferred from the analysis of the available waveforms. Predictor variables have to account for most of the source and propagation effects that can modify the expected value of the selected response variable.

In this study, we simulate different datasets of peak-ground velocities for different structural models with the aim of reproducing a real case where field operations can alter the status of the reservoir. We select a reference GMPE model and next we re-estimate its coefficients to test whether and how they are sensitive to the variations induced in the medium.

The idea of the present analysis is supported by empirical analyses that recognize the need of regionalizing the GMPE in terms of anelastic attenuation in addition to the geometrical attenuation to avoid, for example, an overestimation of the residual standard deviation (Atkinson and Morrison 2009; Kale et al. 2015; Kotha et al. 2016) and by theoretical studies that demonstrate how peak-ground motion parameters and peak frequency parameters are related to earthquake stress-drop, geometrical spreading and anelastic attenuation (Baltay et al. 2013; Lior and Ziv 2018; Wandycz et al. 2019). It is thus possible to think of an inverse procedure that allows to infer stress-drop or anelastic attenuation from peak-ground motion parameters (e.g., Lior and Ziv2018).

We notice that the proposed approach is intended as work in progress that can be used together with well-established techniques for induced seismicity monitoring.

Method

We perform a synthetic test that reproduces the expected seismic activity (seismicity rate, minimum and maximum magnitude, etc.,…) induced by a fluid injection experiment and recorded at a local seismic network. To simulate the variation of the propagation medium properties during the field operations, for each earthquake the waveforms are computed by modifying physical parameters of the propagation medium and in particular the quality factor Q.

The first analysis is devoted to test the difference between a constant Q and a frequency dependent Q. To this aim, we compute synthetic three-component waveforms at 16 stations deployed on an area of 4×4 km^2 (Fig. 1), for 10 hypocentral depths (1.0, 1.25, 1.5, 1.75, 2.0, 2.25, 2.5, 2.75, 3.0, and 3.25) km, a range of hypocentral distances (1, 6.2) km, a range of magnitude (0.0, 3.0) and a homogeneous crustal model ($V_P = 4500$ m/s, $V_S = 2300$ m/s, density $\rho = 2400$ kg/m^3). Earthquakes' depth and stations' location are selected to approximately reproduce a real case of reservoir stimulation where medium properties variation is limited to a relatively

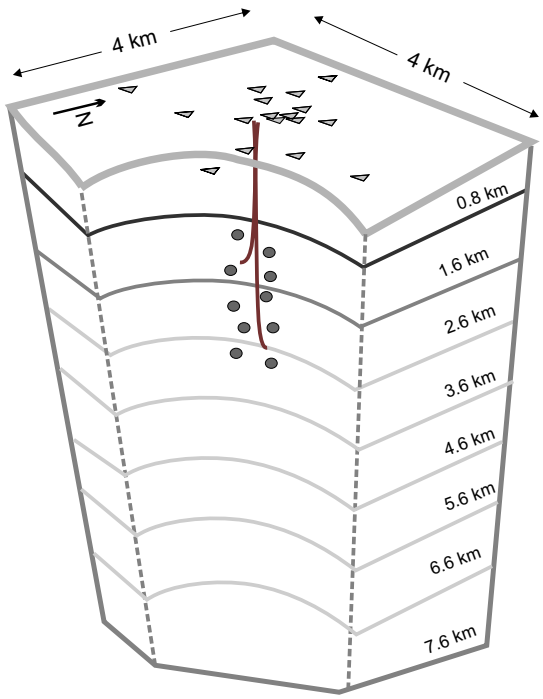

Fig. 1 Sketch of the hypothesized fluid injection experiment. Grey triangles identify the seismic stations, dots the location of the earthquakes. Location and extension of the wells is also indicated together with the depth of the layers

small volume surrounding an injection well (e.g., Soultz-Sous- Forêts, (Alsace, France); Calò and Dorbath 2013).

For the first test, the activity rate is assumed to be constant ($N_{events} = 800$) while individual magnitude values are randomly selected from the Gutenberg–Richter relation assuming a constant b value equal to 1.0.

In order to simulate full-waveforms, we compute the Green's functions by using the code AXITRA (Cotton and Coutant 1997), based on the discrete wavenumber method for a 1D-layered model and a triangle source-time function to represent the earthquake source. In order to set the proper duration of the triangle, we use the Brune's source model (Brune 1970) and, for each magnitude value, we assign a stress-drop value by using an empirical relationship based on the results obtained by Lengliné et al. (2014) for Soultz-Sous-Forêts.

To further increase data heterogeneity, in addition to magnitude, stress-drop and anelastic attenuation, we simulate waveforms of earthquakes taking also into account the different focal mechanisms. In particular, focal mechanisms are selected in the range: strike (140°, 180°), dip (40°, 70°) and rake (− 100°, − 80°) in accordance with an assumed regional stress-field at Soultz-Sous-Forêts (Valley and Evans 2007).

We compute synthetic waveforms for three different decreasing constant Q values ($Q = 160$, 80 and 50) and the final PGV corresponds to the maximum velocity measured on the vector composition of the three-component seismograms. These values are compatible with Q quality factors observed in sedimentary rock reservoirs (Abercrombie 1998; Ripperger et al. 2009; Bethman et al. 2012; Hutchings et al. 2019 and references therein), and with laboratory measurements (e.g., Toksoz et al. 1979; Johnston et al. 1979). However, in the most general formulation of the anelastic attenuation model, Q is frequency dependent and should be written as $Q(f) = Q_o(f/f_o)^n$ where f_o is a reference frequency generally assumed to be 1 Hz (e.g., Morozov 2008) and Q_o is the quality factor Q value at f_o. Thus, to study the effect of the $Q(f)$ models, the results obtained by using the Q-constant values are compared with those obtained for three frequency dependent Q models. For the latter, we use the model $Q(f) = (Vs/32)f^{0.57} = Q_0 f^{0.57}$ presented by Satoh (2004). Specifically, to introduce a frequency-dependent anelastic attenuation, we convolved the Fourier amplitude spectra of the waveforms obtained by using the previous crustal model ($V_P = 4500$ m/s, $V_S = 2300$ m/s, density $\rho = 2400$ kg/m3) without anelastic attenuation, with the $A(R, f) = A_o e^{-\pi f R/Vs Q(f)}$ function. In the previous equation, A_o is the amplitude at the source, f is the frequency, R is the hypocentral distance, V_S is the shear-wave velocity.

We select three different models, $Q(f) = 72f^{0.57}$, $Q(f) = 20f^{0.57}$ and $Q(f) = 10f^{0.57}$. The selection of the specific $Q(f)$ models is done to make them compatible with the constant Q-values in the frequency band (8, 20) Hz, which is the range of interest commonly used to study events (natural and induced) in the magnitude range adopted in the present study (e.g., Emolo et al. 2011; Douglas et al. 2013; Sharma et al. 2013).

Moreover, given the range of distances (1, 6.2) km the peak-ground velocities are measured on S-waves; it is thus reasonable to assume that PGVs are affected by Q_S. Furthermore, since it is expected that Q_P is larger than Q_S (e.g., Lay and Wallace 1995), for simplicity in the waveforms simulation we assume that $Q_P = Q_S$ for each model.

The subsequent analysis is aimed at testing the proposed procedure on a layered crustal model. Given the same network geometry used in the previous analysis, we compute synthetic waveforms and relative PGV values for the three crustal models described below, that mimic the effects of increasing field operations. As for the selection of the layers thickness, velocity and density values we refer to the model proposed by Cuenot et al. (2008) and Valley and Evans (2007) for Soultz-sout-Forêts. We assume that the field operations affect all the layers but that the highest attenuation is attained in the first two layers that could represent the sedimentary sequence. In order to imitate real-data acquisition as much as possible, for each model, we generate a new earthquake catalog assuming a specific b-value. Indeed, it is expected that the b-value changes in space and time during fluid injection operations, deviating from the usually observed $b = 1$ value (Henderson et al. 1999; Cuenot et al. 2008; Convertito et al. 2012; Bachmann et al. 2012), although the variation is not strictly correlated with the injection rate and distance from the well (e.g., Cuenot et al. 2008; Bachmann et al. 2012). For the analysis of the layered crustal models, we assume that the b-value increases as function of the injection rate and moves from a starting value 1 to 1.2 and 1.5 in the last stage of the operations as observed during the hydraulic stimulation at Soultz-sout-Forêts (Cuenot et al. 2008) or during gas depletion in the Netherlands (Van Wees et al. 2014). Similarly, we consider that also the seismicity rate varies during the operations and, in particular, we select 400 events for the first model, 800 events for the second model, and 1200 events for the third model.

For both the two above-mentioned analyses, the PGVs (corresponding to the maximum velocity measured on the vector composition of the three-component seismograms) are measured on the synthetic waveforms for inferring the coefficients of the GMPE using the Levenberg–Marquardt least squares algorithm (Marquardt 1963) for curve fitting.

As a first task for a homogeneous, isotropic medium, we have to select a GMPE, which is assumed as the reference model. For the analyses presented in this study, we select a GMPE with a formulation as simple as possible:

$$\log Y = a + bM + c\log R + dR \quad (1)$$

where Y is the PGV, R is the hypocentral distance and M is the earthquake magnitude. In Eq. (1), the coefficients a and b account for the effect of the earthquake size on Y, while c accounts for the geometrical spreading, and d accounts for the anelastic attenuation, which represents the fractional loss of energy for cycle of oscillation during wave propagation (e.g., Knopoff 1964; Del Pezzo and Bianco 2013). As reported above, the intrinsic anelastic attenuation is inversely related to the quality factor Q (Knopoff 1964) and can be modeled as a filter of the form $A(R,f) = A_o e^{-\pi f R/VsQ}$, which is thus convolved with the source spectrum (Babaie Mahani and Atkinson 2012). We notice that, as reported by Cotton et al. (2008), the interpretation of the term dR as the anelastic attenuation effect in the GMPE is only strictly correct when considering Fourier amplitudes for a particular frequency. However, since PGVs are measured at the amplitude spectral peak and this latter has a bell-shape (if a ω^{-2} displacement spectral model is assumed) modified by the anelastic effect, which always shifts the corner frequency toward lower values, we can assume that PGVs are associated to a limited frequency range. The GMPE is also associated with an error $\sigma_{\log Y}$ corresponding to the total standard error, describing uncertainty in the value of Y given the predictive relationship.

Equation (1) represents a simple model compared to many formulations with higher degree of complexity (e.g., Douglas 2003; Douglas et al. 2013) that could better account for the physical processes affecting the recorded ground motion parameter. However, additional terms accounting for nonlinearity in magnitude scaling and magnitude-dependent geometrical spreading are effective and can be resolved for distances and magnitudes larger than those considered in this study (Bommer et al. 2007; Cotton et al. 2008; Baltay and Hanks 2014).

To infer the reference model, we simulated 800 events using the stations' configuration and earthquakes depths' distribution described above. As for the initial Q we refer to Charléty et al. (2007) and Beauce et al. (1992) who suggest that Q_S is about 500 in the granite and a minimum value of 50 in the upper sedimentary layers.

The approach proposed in this study is to use the earthquakes recorded during the field operations to infer and/or update the coefficients a, b, c and d (De Matteis and Convertito 2015) and test which of them have to be analyzed to monitor the status of the reservoir. In particular, we test two cases. In the first case, all the earthquakes recorded during a fixed period are used to infer the new coefficients. A similar approach has been used by Chiou and Youngs (2008) to study the dependence of the anelastic attenuation term on the magnitude. In the second case, data of synthetic earthquakes are individually used to infer the new coefficients. This analysis was designed to be applied, for example, during those stages of field operations when earthquakes do not occur continuously over time and are not enough numerous to update all the coefficients of a reference model. However, we verified that the analysis of single events could still provide information on any critical change in the medium.

Results and conclusion

The dataset used to infer the reference model (MODREF) reported in Eq. (1) is shown in Fig. 2 and the obtained coefficients are listed in Table 1. In addition to the normality plot shown in Fig. 2d, we performed the analysis of variance (ANOVA) (Fisher 1990), which allows to test the null hypothesis that the coefficients in regression model are zero against the alternative hypothesis that the coefficients are different from zero. It can be shown that the test statistic has an $F(p, n-p-1)$ distribution where p is the number of parameters to be inferred and n is the number of data (Fisher 1990). We note that the F test does not indicate which of the parameters is not equal to zero, but only that at least one of them is linearly related to the response variable. The result of the ANOVA for MODREF is reported in Table 2 and, based on the computed p value (<0.0001) we cannot accept the null hypothesis that coefficients are zero at 95% level of confidence. Moreover, the obtained $R^2 = 0.897$ indicates that about 90% of the variation of the response variable is explained by the predictive variables.

The initial analysis is devoted to study the effect of considering Q constant quality factor *vs* Q frequency-dependent quality factor. To this aim, we compute the updated coefficients of Eq. (1) using PGVs simulated for models with $Q = 160$, 80 and 50 that are compared with $Q(f) = 72f^{0.57}$, $20f^{0.57}$ and $10f^{0.57}$, respectively. The results are depicted in Fig. 3 while the coefficients are listed in Table 3. It is noticeable how the GMPE coefficients show a similar variation

Table 1 Coefficients and relative uncertainties of the GMPEs obtained by analyzing PGVs corresponding to the reference crustal model and to MOD1, MOD2 and MOD3

MODEL	a	b	c	d	$\sigma_{\log Y}$
MODREF	-5.309 ± 0.005	0.950 ± 0.003	-1.32 ± 0.04	-0.0197 ± 0.0059	0.170
MOD1	-5.312 ± 0.008	0.928 ± 0.005	-1.17 ± 0.06	-0.0253 ± 0.0084	0.171
MOD2	-5.371 ± 0.005	1.023 ± 0.004	-1.10 ± 0.04	-0.0803 ± 0.0058	0.168
MOD3	-5.434 ± 0.004	1.188 ± 0.004	-1.17 ± 0.03	-0.1204 ± 0.0046	0.162

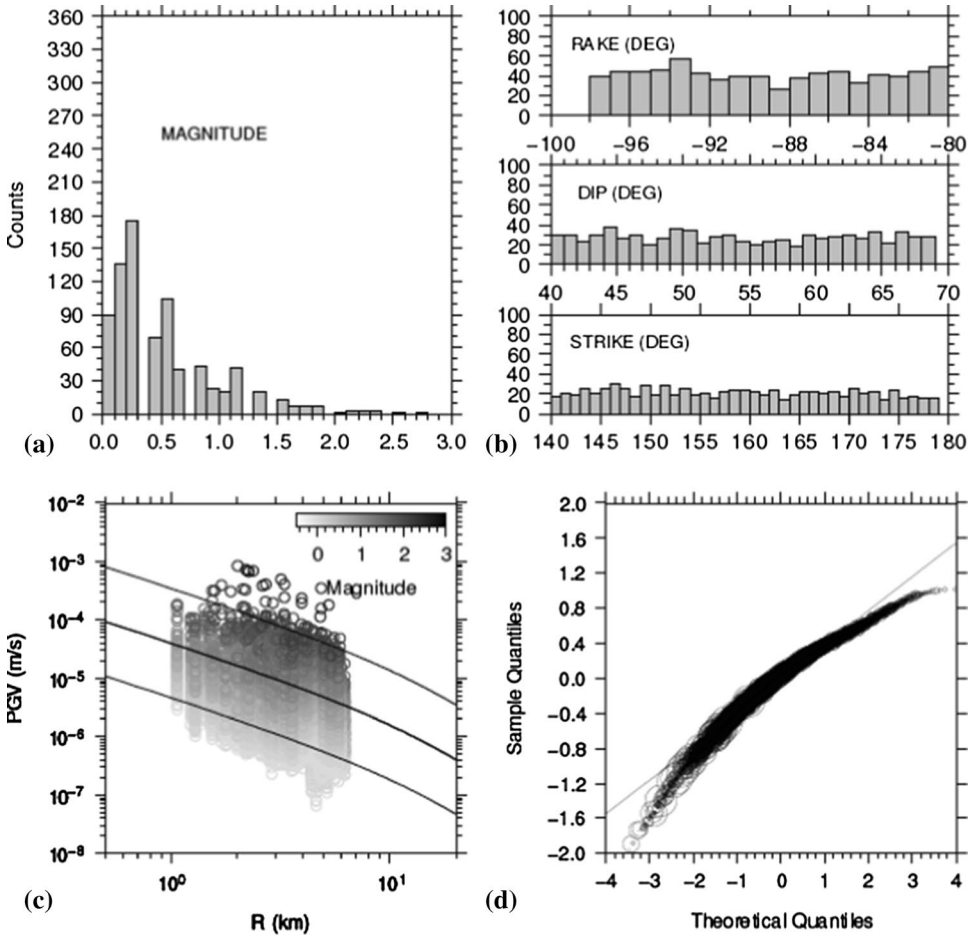

Fig. 2 **a** Magnitude distribution for the catalogue used to infer the reference model (MODREF). **b** Sample distribution of the focal mechanism angles (strike, dip and rake) for the same catalogue. **c** PGVs as function of distance used to infer MODREF. Circles are color coded according to the magnitude of the earthquake. The black lines correspond to the inferred GMPE computed for magnitude values *M* 0, 1 and 2. **d** Normality plot for the residuals. The dimension of the circles is proportional to the event's magnitude

Table 2 ANOVA table for the GMPE relative to the reference model MODREF. The value of the squared multiple correlation coefficient R^2 is also reported

Source	SS	*df*	MS	*F*	*p* value
SSR	17,208.5234	4	MSR = 4302.13086	27,988.4453	< 0.001
SSE	1966.73181	12,795	MSE = 0.153710961		
SST	19,175.2051	12,799			

$R^2 = 0.897436202$

SST sum of squares total, *SSR* sum of squares regression, *SSE* sum of squares error, *np* number of parameters, *n* number of data, *df* degree of freedom, *F* F-statistic

$p = P(Fn_{p,n-np-1} > F^*)$

MSE (= SSE/$n - np - 1$): Mean square error

MSR (= SSR/np): Mean square regression

regardless of using a frequency dependent or a constant attenuation model and, in particular, the *d* coefficient is sensitive to the variations of *Q*, decreasing with the increase in the anelastic attenuation. Thus, for the following analysis we can adopt the *Q* constant models.

Next, to simulate a more reasonable propagation medium with respect to a homogeneous medium, we analyze PGVs data simulated by using the three-layered models reported in Table 4 (MOD1, MOD2 and MOD3). Incidentally, we notice that the *Q* value in the first layer in MOD3 is a value generally measured in the first 100 m (Abercrombie, 1998) that we arbitrarily extrapolated up to 800 m only to test an extreme case. The simulated datasets for MOD1, MOD2 and MOD3 are shown in Figs. 4, 5 and 6, respectively, while the inferred coefficients are listed in Table 1. For each regression, we performed the ANOVA whose results are listed in Tables 5, 6 and 7. Also for the layered models, the ANOVA indicates that the hypothesis of zero value coefficients cannot be accepted and that R^2 is larger than 88%.

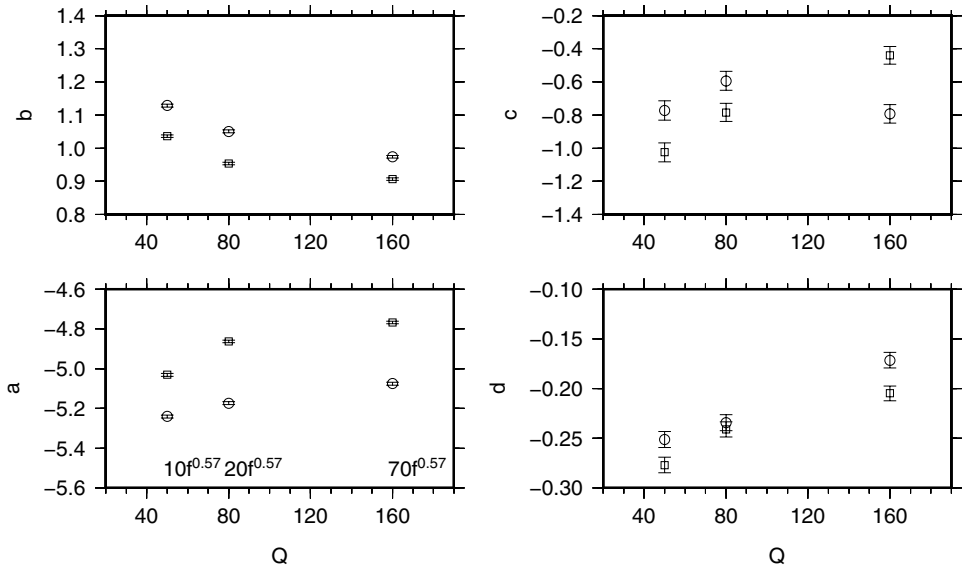

Fig. 3 Result of the test aimed at comparing the coefficients inferred for constant Q models (160, 80 and 50) (circles) with those computed for Q frequency-dependent models (squares) ($Q = 10f^{0.57}$, $20f^{0.57}$ and $70f^{0.57}$)

Table 3 Coefficients and relative uncertainties of the GMPEs obtained by analyzing PGVs corresponding to the selected constant Q models and those relative to the Q frequency-dependent models

Q		a	b	c	d	$\sigma_{\log Y}$
160	QC1	− 5.076 ± 0.007	0.974 ± 0.004	− 0.79 ± 0.05	− 0.172 ± 0.008	0.233
$72f^{0.57}$	QF1	− 4.768 ± 0.007	0.907 ± 0.004	− 0.44 ± 0.05	− 0.205 ± 0.007	0.229
80	QC2	− 5.174 ± 0.007	1.051 ± 0.004	− 0.59 ± 0.06	− 0.234 ± 0.008	0.239
$20f^{0.57}$	QF2	− 4.865 ± 0.007	0.954 ± 0.004	− 0.78 ± 0.05	− 0.241 ± 0.008	0.230
50	QC3	− 5.241 ± 0.007	1.128 ± 0.004	− 0.77 ± 0.06	− 0.251 ± 0.008	0.245
$10f^{0.57}$	QF3	− 5.031 ± 0.008	1.036 ± 0.004	− 1.20 ± 0.06	− 0.277 ± 0.008	0.236

Table 4 Structural models used to simulate waveforms and the relative PGVs shown in Figs. 4, 5 and 6. Z is the depth of the layers, V_P and V_S refers to P- and S-wave velocity, ρ is the density and Q_P and Q_S the P and S quality factors. The last three columns report the three investigated anelastic models: MOD1, MOD2 and MOD3

Z (m)	V_P (m/s)	V_S (m/s)	ρ (kg/m^3)	Q_P, Q_S	Q_P, Q_S	Q_P, Q_S
0.0	1850	860	2000	50	20	10
800	2870	1340	2200	100	50	25
1600	5800	3310	2600	500	100	50
2600	5820	3320	2600	500	100	50
3600	5850	3340	2600	500	100	50
4600	5870	3350	2600	500	100	50
5600	5900	3370	2600	500	100	50
6600	5920	3380	2650	500	100	50
7600	5950	3400	2650	500	100	50

From the analysis of Table 1, we note that the inferred d coefficient decreases with the decreasing of the quality factor, that is, when the attenuation is higher. The decrease in the standard deviation from MOD1 to MOD3 is likely due to the increase in the b-value of the Gutenberg–Richter relation used in our simulations. In particular, higher b values correspond to a higher percentage of smaller magnitude events, which are similarly affected by the anelastic attenuation compared to the case in which a wider range of magnitude (i.e., lower b value) is considered. In order to analyze the differences between the inferred d coefficients, we use a Student's t test at 95% level of significance. The results indicate that the difference between the d values is statistically significant (see Table 8). In addition, for each investigated model we report in Fig. 7 the distribution of residuals ($\log PGV^{obs} - \log PGV^{pred}$) as function of distance and magnitude. A regression analysis indicates that for all the considered GMPEs there is no trend in the residuals as function of distance. This means that all the models properly account for the geometrical and anelastic attenuation.

In order to test the resolution of the proposed technique, we modified MOD2 by decreasing the Q values by 30%

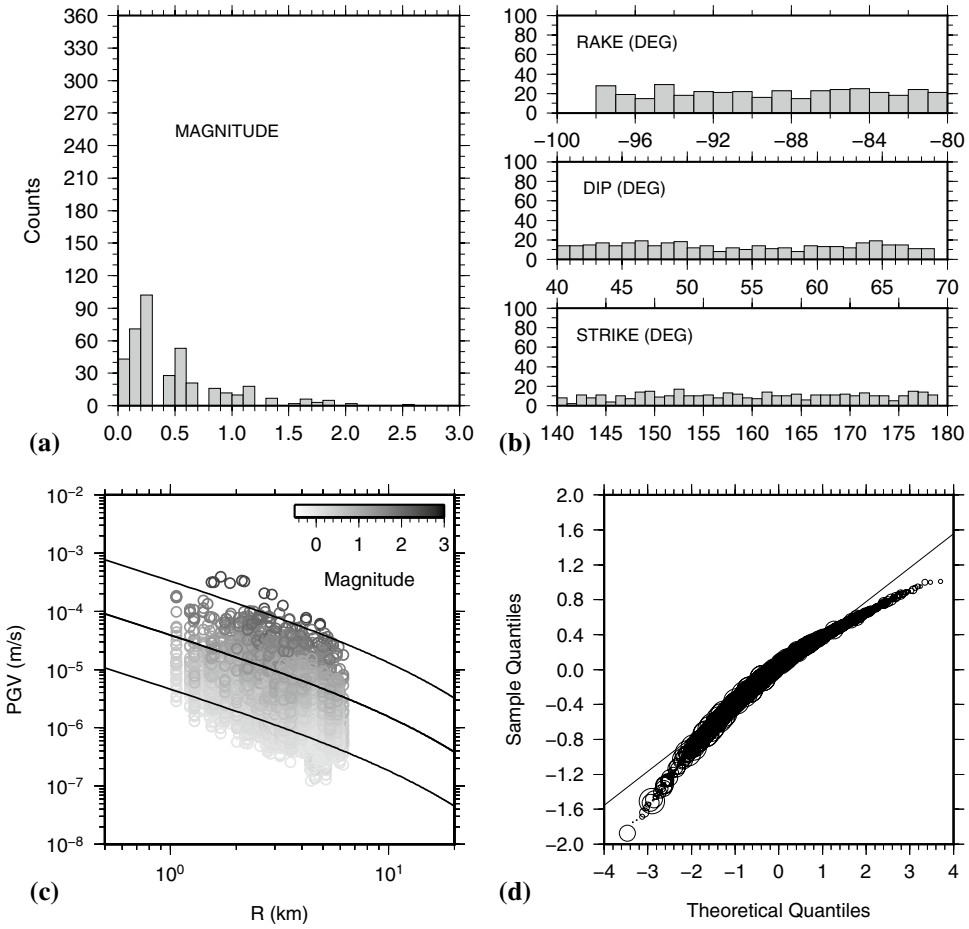

Fig. 4 Same as Fig. 2 but for MOD1

(MOD2P30) and 20% (MOD2P20). We note that MOD3 is obtained by reducing Q of MOD2 by 50% and that for MOD3 the t test reported in Table 8 has shown a statistical difference. The coefficients obtained for the modified models are listed in Table 9 while Table 10 reports the result of the t test aimed at verifying the statistical difference between the inferred d values. The test indicates that the d values are statistically different and thus the approach presented in this study can resolve variation of Q in the order of 20%. Lower variations seem to be unfeasible because they would be lower than the uncertainty generally associated with the estimation of Q for real data (White 1992).

The last application concerns the case when data of each earthquake are separately inverted. We note that, when analyzing a single earthquake there is an intrinsic difficulty to infer all the parameters of the GMPE due to the limited number of data.

Preliminary tests have shown that both b and c parameters must be set equal to the reference values ($b = b_{ref}$, $c = c_{ref}$) while inverting a and d. A similar result is obtained when the number of earthquakes is not enough to build a homogenous PGVs dataset.

This assumption means that operations do not strongly affect the geometrical spreading of the S-waves travelling from the source to the receivers and that the same operations only partially affect the earthquakes stress-drop. Concerning the assumption about the geometrical spreading we note that, while it is a reasonable assumption for conventional filed operation, it could not be fully valuable for fracking operations (e.g., Adachi et al. 2007; Belyadi et al. 2019). As for the stress drop, while the variation generally observed for natural moderate-to-large earthquakes spans over at least 4 order of magnitude (e.g., Allman and Shearer 2009), the one observed for induced seismicity falls within a tighter range of values (e.g., Goertz-Allmann et al. 2011; Lengliné et al. 2014; Martínez-Garzón et al. 2014; Staszek et al. 2017). The results of the analysis are shown in Fig. 8 and indicate a clear variation of the coefficient d when moving from MOD1 to MOD3, that is, when the anelastic attenuation is increased. This finding still holds when a random noise (in the range ± 40% of PGV at each station) is added to the simulated PGVs.

Moreover, for each crustal model there is an evident variation of d when data from low magnitude events are inverted. This can be explained by considering that the

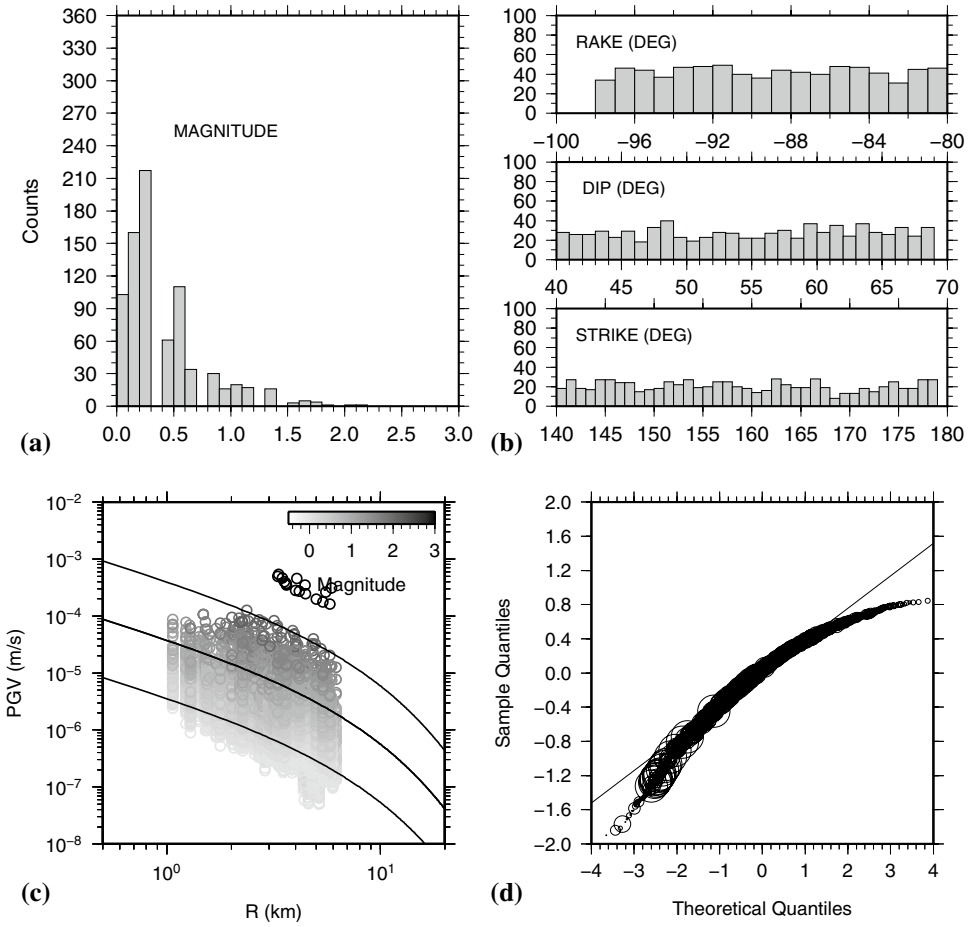

Fig. 5 Same as Fig. 2 but for MOD2

observed velocity spectrum can be modeled as the product of two terms $S(f)$ and $A(R, f)$. The term $S(f) = 2\pi f\, \Omega_o/(1 + (f/f_c)^2)$ is the source spectrum, where Ω_o is the low-frequency spectral level from which seismic moment can be computed and f_c is the corner frequency. The term $A(R,f) = A_o e^{-\pi f R/V_s Q}$ is the attenuation spectrum model. If one assumes that PGV is measured at the maximum of the amplitude spectrum it can be shown that, at a given distance from the source, the effect of the anelastic attenuation is larger for smaller magnitude events that have higher corner frequencies compared to larger magnitude events.

The conclusions of the present study can be summarized as follows:

- GMPEs can be used to observe the variations of Q during field operations. When a large dataset is available, all the coefficients of the GMPE can be inverted and compared with those of a reference model to check if significant variations (from a statistical point of view) of the coefficients are occurring. However, preliminary tests have shown that, when the dataset is not homogeneous in terms of magnitude and distances, as for the case of the initial phases of a project (e.g., first stimulation of reservoir, acidifications) some of the coefficients must be set to *a-priori* selected values.
- As a consequence of the above conclusion, the proposed approach cannot be applied when field operations strongly affect the geometrical spreading, as in the case of fracking operations, or produce a variation in the stress-drop larger than 3 to 4 order of magnitude. In fact, these large variations cause that the coefficient b or c cannot be set to *a-priori* constant values.
- Aside from the possibility of inverting all the coefficients of the GMPE (as in the case when all the events are inverted together) or the necessity of fixing some of them, as in the case of the analysis of single earthquakes, the synthetic tests presented in this study have shown that the coefficient d is statistically sensitive to the anelastic attenuation variations.
- The tests indicate that the variation of d due to anelastic attenuation dominates the variations possibly due to focal mechanisms, stress-drop and magnitude. Indeed, since in each simulation we have imposed the same variation of the focal parameters, if the focal mechanisms would have dominated the PGV amplitudes variation, the d coefficients would not have changed.

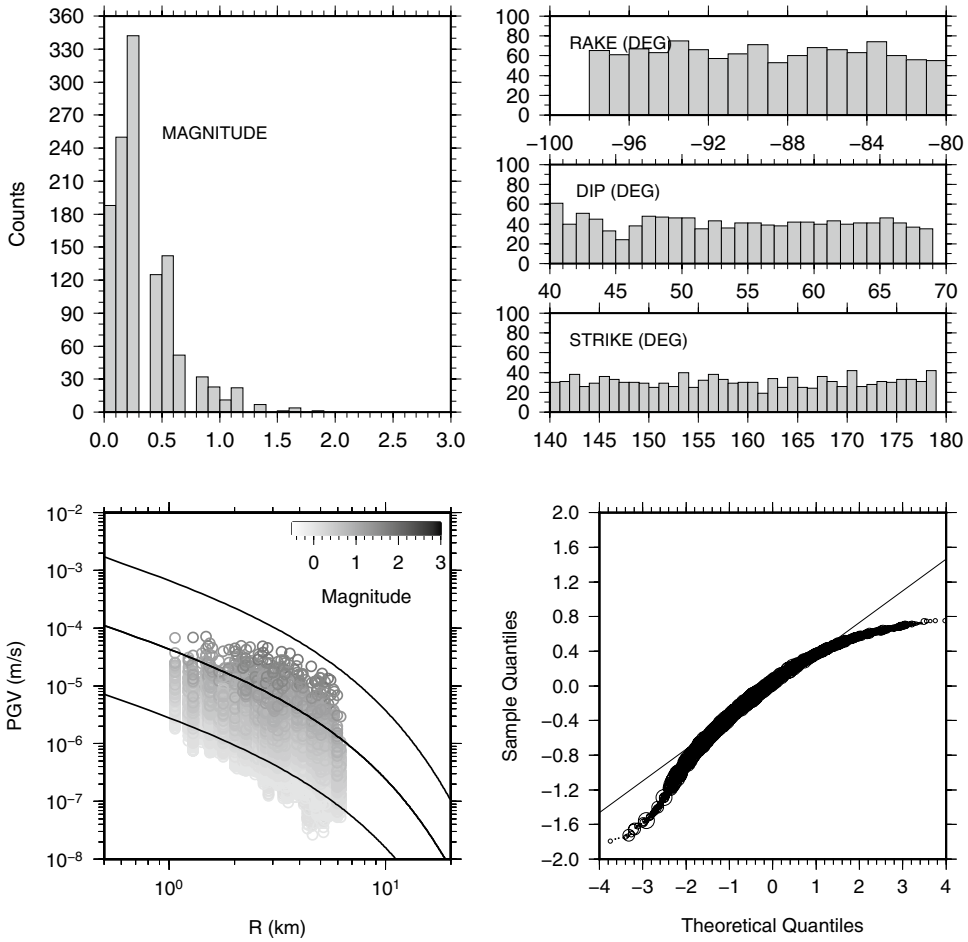

Fig. 6 Same as Fig. 2 but for MOD3

Table 5 ANOVA table for MOD1

Source	SS	*df*	MS	*F*	*p* value
SSR	7516.392	4	1879.098	12,086.59	< 0.0001
SSE	994.228	6395	0.1551		
SST	8510.620	6399			

See Table 2 for details. $R^2 = 0.883$

Table 6 ANOVA table for MOD2

Source	SS	*df*	MS	*F*	*p* value
SSR	15,414.262	4	3853.565	25,849.76	< 0.0001
SSE	1907.420	12,795	0.149		
SST	17,321.625	12,799			

See Table 2 for details. $R^2 = 0.890$

Table 7 ANOVA table for MOD3

Source	SS	*df*	MS	*F*	*p* value
SSR	23,208.998	4	5802.249	41,486.89	< 0.0001
SSE	2684.563	19,195	0.140		
SST	25,893.496	19,199			

See Table 2 for details. $R^2 = 0.896$

Table 8 Observed values of the statistic *t* to compare with the critical values $t_c = \pm 1.96$ and the corresponding computed *p* value

MOD	NPGVs	*t* statistic	*p* value
MODREF MOD1	12,800–6400	– 15.328	< 0.0001
MOD1 MOD2	6400–12,800	– 530.009	< 0.0001
MOD2 MOD3	12,800–9200	– 605.894	< 0.0001

- The analysis of single earthquakes suggests that, for each used crustal model, coefficients' variation is more evident when the analysis is done for single, small magnitude earthquakes.
- The proposed technique has the advantage that it requires only the location of the event and the measure of the PGVs that, compared to other measures such as P- and S-wave picking (necessary to imple-

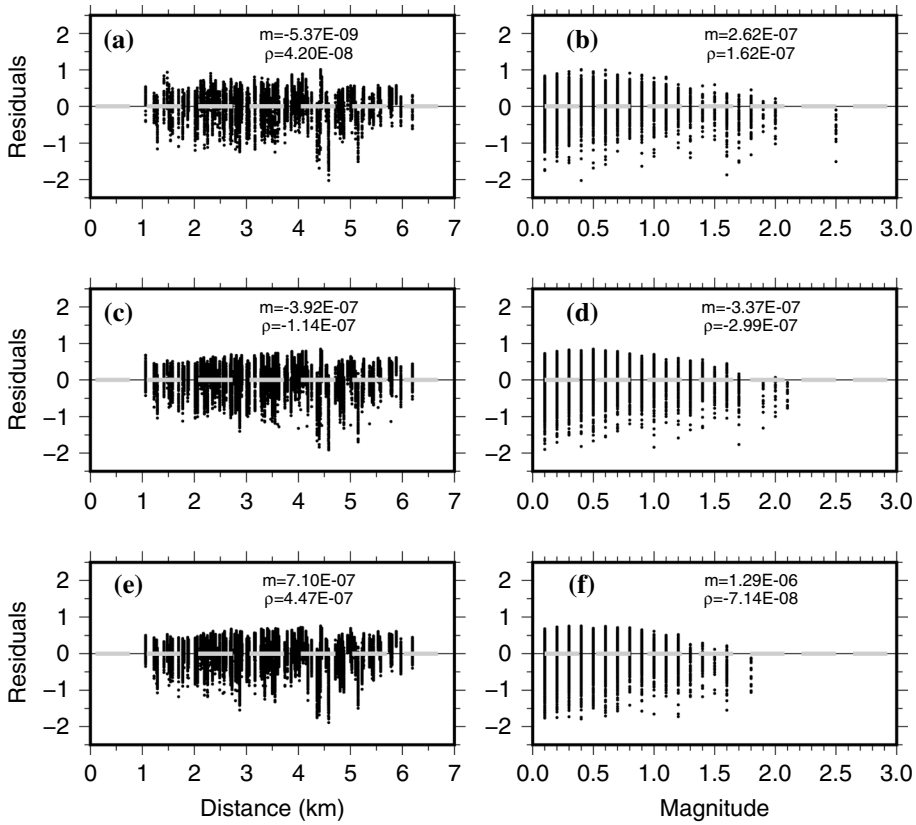

Fig. 7 Residuals as function of distance and magnitude. **a**, **b** Refer to MOD1. **c**, **d** Refer to MOD2 and **e**, **f** refer to MOD3. The coefficients m and ρ reported in each panel indicate the slope of the best-fit line (gray dashed line) and the linear correlation coefficient, respectively

Table 9 Coefficients and relative uncertainties for the resolution analysis

MODEL	*a*	*b*	*c*	*d*	$\sigma_{\ln Y}$
MOD2P30 (30%)	− 5.398 ± 0.005	1.064 ± 0.004	− 1.11 ± 0.04	− 0.0974 ± 0.0057	0.165
MOD2P20 (20%)	− 5.376 ± 0.005	1.034 ± 0.004	− 1.08 ± 0.04	− 0.0956 ± 0.0057	0.166

The coefficients refer to the GMPEs obtained by analyzing PGVs when the anelastic attenuation in MOD2 is decreased by 30% and 20%, respectively

Table 10 Observed values of the statistic *t* to compare with the critical values $t_c = \pm 1.96$, the corresponding computed *p* value and the number of PGVs used to test the resolution of the proposed technique. The coefficients of the GMPEs are listed in Table 9

MOD	NPGVs	*t* statistic	*p* value
MOD2 MOD2P20	12,800–12,800	− 212.862	< 0.0001
MOD2P20 MOD2P30	12,800–12,800	25.043	< 0.0001
MOD2P30 MOD3	12,800–19,200	− 394.146	< 0.0001

ment tomographic approaches) or P-wave pulse width measure (e.g., Zollo and de Lorenzo 2001) or the peak frequency (e.g., Wandycz et al. 2019) are more readily measured after the earthquake occurrence.

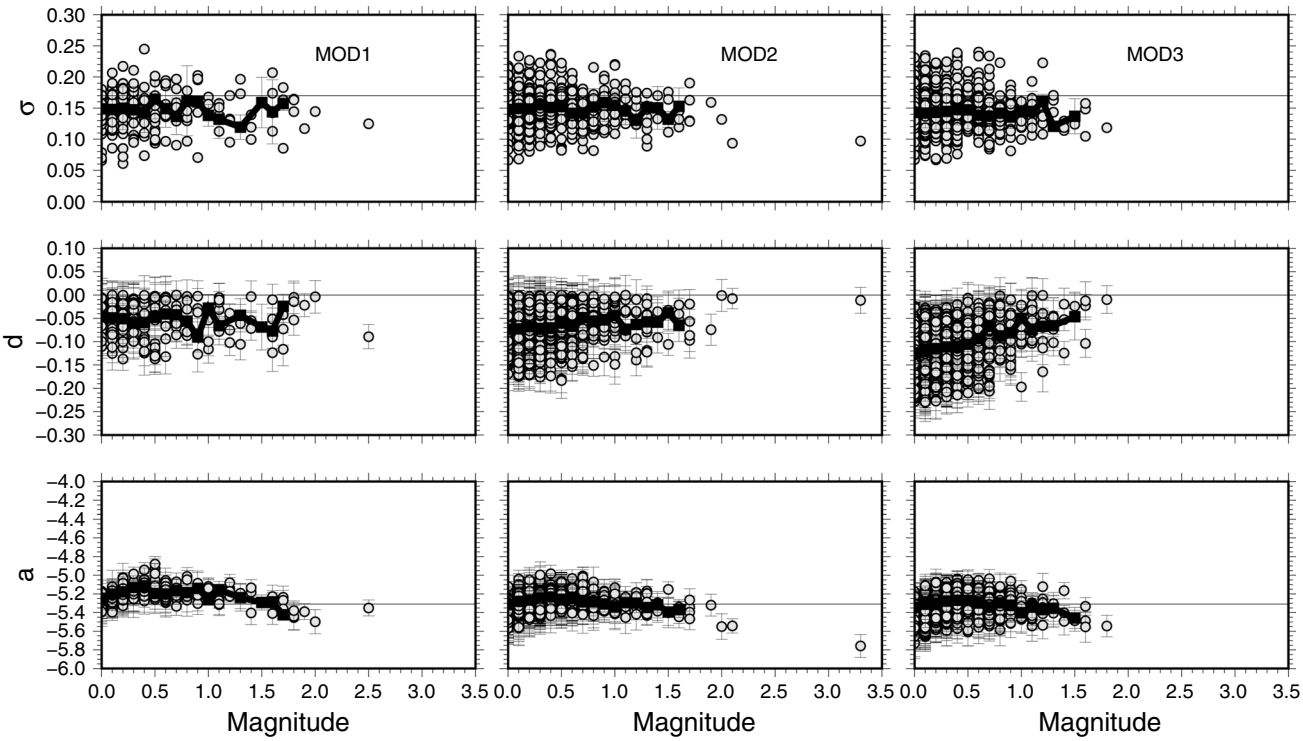

Fig. 8 Results of the sensitivity test of the coefficients of the GMPE when data of each earthquake are separately inverted. The coefficients are shown as function of the magnitude for the three investigated models listed in Table 4. Data used to infer the coefficients are those reported in Figs. 4, 5 and 6, respectively corresponding to MOD1, MOD2 and MOD3. Black squares correspond to the mean value (computed by binning the magnitude values) of the parameter while the horizontal lines correspond to the reference value of the parameter

Data and resources

Figures have been generated with the Generic Mapping Tools (GMT; Wessel and Smith 1991). S4CE (Science for Clean Energy) supporting project details can be found at www.science4cleanenergy.eu.

Acknowledgements The authors wish to thank the associated Editor Prof. Lasocki and two anonymous reviewers whose comments and suggestions helped to improve the manuscript. This study was carried out within the framework of the S4CE (Science for Clean Energy) project, which received funding from the European Union's Horizon 2020 research and innovation action, under grant agreement No 764810, and was partially funded by the PRIN Project MATISSE (Bando 2017, Prot. 20177EPPN2).

Compliance with ethical standards

Conflict of interest On behalf of all authors, the corresponding author states that there is no conflict of interest.

References

Abercrombie RE (1998) A summary of attenuation measurements from borehole recordings of earthquakes: the 10Hz transition problem. Pure Appl Geophys 153:475–487

Adachi J, Siebrits E, Peirce A, Desroches J (2007) Computer simulation of hydraulic fractures. Int J Rock Mech Min Sci 44(5):739–757

Allmann BP, Shearer PM (2009) Global variations of stress drop for moderate to large earthquakes. J Geophys Res 114:B01310. https://doi.org/10.1029/2008JB005821

Atkinson GM, Morrison M (2009) Observations on regional variability in ground-motion amplitudes for small-to-moderate earthquakes in North America. Bull Seismol Soc Am 99:2393–2409

Babaie Mahani A, Atkinson GM (2012) Evaluation of functional forms for the attenuation of small-to-moderate earthquake response spectral amplitudes in North America. Bull Seismol Soc Am 102:2714–2726

Bachmann CE, Wiemer S, Goertz-Allmann BP, Woessner J (2012) Influence of pore-pressure on the event-size distribution of

induced earthquakes. Geophys Res Lett 39:L09302. https://doi.org/10.1029/2012GL051480
Baltay AS, Hanks TC, Beroza GC (2013) Stable stress-drop measurements and their Variability: Implications for Ground-Motion Prediction. Bull Seismol Soc Am 103:211–222
Baltay AS, Hanks TC (2014) Understanding the magnitude dependence of PGA and PGV in NGA-West2 Data. Bull Seis Soc Am 104:6. https://doi.org/10.1785/0120130283
Beauce A, Fabriol H, Le Masne D, Cavoit C, Mechler P, Chen XK (1992) Seismic studies on the HDR site of Soultz-sous-Forets (Alsace, France). In: Bresee JC (ed) Geothermal energy in Europe: the Soultz Hot Dry Rock project. Routledge, London
Belyadi H, Fathi E, Belyadi F (2019) Chapter Fifteen—Numerical simulation of hydraulic fracturing propagation. In: Hydraulic fracturing in unconventional reservoirs. Theories, operations, and economic analysis (2nd Edn), Elsevier, Amsterdam, pp 257–272
Bethmann F, Deichmann N, Mai PM (2012) Seismic wave attenuation from borehole and surface records in the top 2.5 km beneath the city of Basel, Switzerland. Geophys J Int 190:1257–1270. https://doi.org/10.1111/j.1365-246X.2012.05555.x
Bommer JJ, Stafford PJ, Alarcón JE, Akkar S (2007) The influence of magnitude range on empirical ground-motion prediction. Bull Seismol Soc Am 97:2152–2170. https://doi.org/10.1785/0120070081
Brune J (1970) Tectonic stress and the spectra of seismic shear waves from earthquakes. J Geophys Res 75:4997–5009
Calò M, Dorbath C (2013) Different behaviours of the seismic velocity field at Soultz-sous Forêts revealed by 4D seismic tomography: case study of GPK3 and GPK2 injection tests. Geophys J Int 194(2):1119–1137. https://doi.org/10.1093/gji/ggt153
Chiou B, Youngs RR (2008) An NGA model for the average horizontal component of peak ground-motion and response spectra. Earthq Spectra 24:173–216
Charléty J, Cuenot N, Dorbath L, Dorbath C, Haessler H, Frogneux M (2007) Large earthquakes during hydraulic stimulations at the geothermal site of Soultz-sous-Forêts. Int J Rock Mech Min Sci 44(8):1091–1105
Convertito V, De Matteis R, Cantore L, Zollo A, Iannaccone G, Caccavale M (2010) Rapid estimation of ground-shaking maps for seismic emergency management in the Campania Region of southern Italy. Nat Hazards 52(1):97. https://doi.org/10.1007/s11069-009-9359-2
Convertito V, Maercklin N, Sharma N, Zollo A (2012) From induced seismicity to direct time-dependent Seismic Hazard. Bull Seismol Soc Am 102(6):2563–2573. https://doi.org/10.1785/0120120036
Cotton F, Coutant O (1997) Dynamic stress variations due to shear faults in a plane-layered medium. Geophys J Int 128(3):676–688. https://doi.org/10.1111/j.1365-246X.1997.tb05328.x
Cotton F, Pousse G, Bonilla F, Scherbaum F (2008) On the discrepancy of recent European ground motion observations and predictions from empirical models: analysis of KiK-net accelerometric data and point-sources stochastic simulations. Bull Seismol Soc Am 98(5):2244–2261
Cuenot N, Dorbath C, Dorbath L (2008) Analysis of the microseismicity induced by fluid injections at the Hot Dry Rock site of Soultz-sous-Forêts (Alsace, France): implications for the characterization of the geothermal reservoir properties. Pure Appl Geophys 165:797–828
Del Pezzo E, Bianco F (2013) A reappraisal of seismic Q evaluated in Campi Flegrei caldera. Receipt for the application to risk analysis. J Seismol 17:829–837. https://doi.org/10.1007/s10950-012-9349-9
De Matteis R, Convertito V (2015) Near-real time ground-motion updating for earthquake shaking prediction. Bull Seismol Soc Am 105(1):400–408. https://doi.org/10.1785/0120140145
Douglas J (2003) Earthquake ground motion estimation using strong-motion records: a review of equations for the estimation of peak ground acceleration and response spectral ordinates. Earth Sci Rev 61:43–104. https://doi.org/10.1016/S0012-8252(02)00112-5
Douglas J, Edwards B, Convertito V, Sharma N, Tramelli A, Kraaijpoel D, Cabrera BM, Maercklin N, Troise C (2013) Predicting Ground Motion from Induced Earthquakes in Geothermal Areas. Bull Seismol Soc Am. https://doi.org/10.1785/0120120197
Emolo A, Convertito V, Cantore L (2011) Ground-motion predictive equations for low-magnitude earthquakes in the Campania-Lucania area, Southern Italy. J Geophys Eng 8:46–60. https://doi.org/10.1088/1742-2132/8/1/007
Fisher RA (1990) Statistical methods, experimental design, and scientific inference. Oxford University Press, Oxford
Giardini D (2009) Geothermal quake risks must be faced. Nature 462:848–849. https://doi.org/10.1038/462848a
Goertz-Allmann BP, Goertz A, Wiemer S (2011) Stress drop variations of induced earthquakes at the Basel geothermal site. Geophys Res Lett 38:L09308. https://doi.org/10.1029/2011GL047498
Grigoli F, Cesca S, Priolo E, Rinaldi AP, Clinton JF, Stabile TA, Dost B, Fernandez MG, Wiemer S, Dahm T (2017) Current challenges in monitoring, discrimination, and management of induced seismicity related to underground industrial activities: a European perspective. Rev Geophys 55:310–340. https://doi.org/10.1002/2016RG000542
Gritto R, Jarpe SP (2014) Temporal variations of V_P/Vs-ratio at the Geysers geothermal field. USA, Geothermics 52:112–211
Guha SK (2000) Induced earthquake. Kluwer Academic Publishers, Dordrecht
Henderson JR, Barton DJ, Foulger GR (1999) Fractal clustering of induced seismicity in the Geysers geothermal area, California. Geophys J Int 139:317–324
Hutchings LB, Bonner S, Saltiel SJ, Nelson M (2019) Rock physics interpretation of tomographic solutions for geothermal reservoir properties in applied geophysics with case studies on environmental. Explor Eng Geophys. https://doi.org/10.5772/intechopen.78490
Johnston DH, Toksoz MN, Timur A (1979) Attenuation of seismic waves in dry and saturated rocks: II. Mech Geophys 44:691–711
Kale Ö, Akkar S, Ansari A, Hamzehloo H (2015) A ground-motion predictive model for Iran and Turkey for horizontal PGA, PGV, and 5 % damped response spectrum: investigation of possible regional effects. Bull Seismol Soc Am 105(2A):963–980
Knopoff L (1964) Solid-earth geophysics. Q Rev Geophys 2:625–660
Kotha SR, Bindi D, Cotton F (2016) Partially non-ergodic region specific GMPE for Europe and Middle-East. Bull Earthq Eng 14(4):1245–1263
Lay T, Wallace TC (1995) Modern global seismology. Academic Press, New York, ISBN #0-12-732870-X
Lengliné O, Lamourette L, Vivin L, Cuenot N, Schmittbuhl J (2014) Fluid-induced earthquakes with variable stress drop. J Geophys Res Solid Earth 119:8900–8913. https://doi.org/10.1002/2014JB011282
Lior I, Ziv A (2018) The relation between ground motion, earthquake source parameters, and attenuation: Implications for source parameter inversion and ground motion prediction equations. J Geophys Res Solid Earth. https://doi.org/10.1029/2018JB015504
López-Comino JA, Cesca S, Jarosławski J, Montcoudiol N, Heimann S, Dahm T, Lasocki T, Gunning A, Capuano P, Ellsworth WL (2018) Induced seismicity response of hydraulic fracturing: results of a multidisciplinary monitoring at the Wysin site Poland. Sci Rep 8:1–14. https://doi.org/10.1038/s41598-018-26970-9

Marquardt D (1963) An algorithm for least-squares estimation of nonlinear parameters. SIAM J Appl Math 11:431–441. https://doi.org/10.1137/0111030

Martínez-Garzón P, Kwiatek G, Sone H, Bohnhoff M, Dresen G, Hartline C (2014) Spatiotemporal changes, faulting regimes, and source parameters of induced seismicity: a case study from the Geysers geothermal field. J Geophys Res 119:8378–8396. https://doi.org/10.1002/2014JB011385

Morozov IB (2008) Geometrical attenuation, frequency dependence of Q, and the absorption band problem. Geophys J Int 172:239–252. https://doi.org/10.1111/j.1365-246X.2008.03888.x

Ripperger J, Kastli P, Fah D, Giardini D (2009) Ground motion and macroseismic intensities of a seismic event related to geothermal reservoir stimulation below the city of Basel—observations and modeling. Geophys J Int 179:1757–1771. https://doi.org/10.1111/j.1365-246X.2009.04374.x

Satoh T (2004) Inversion of S-wave velocity and Qs of deep sediments from surface to borehole spectral ratios considering obliquely incident SH and SV waves. In: Paper presented at the 13 world conference on earthquake engineering, Vancouver, Canada

Sharma N, Convertito V, Maercklin N, Zollo A (2013) Ground motion prediction equation for "The Geysers" geothermal area based on induced seismicity records. Bull Seismol Soc Am 103:117–130. https://doi.org/10.1785/0120120138

Staszek KM, Orlecka-Sikora B, Leptokaropoulos K, Kwiatek G, Martínez-Garzón P (2017) Temporal static stress drop variations due to injection activity at The Geysers geothermal field, California. Geophys Res Lett 44:7168–7176. https://doi.org/10.1002/2017GL073929

Toksoz MN, Johnston DH, Timur A (1979) Attenuation of seismic waves in dry and saturated rocks: I Laboratory measurements. Geophysics 44:681–690

Valley B, Evans K (2007) Stress state at Soultz-Sous-Forêts to 5 km depth from wellbore failure and hydraulic observations. In: Paper presented at thirty-second workshop on geothermal reservoir engineering, Stanford, USA

Van Wees JD, Buijze L, Van Thienen-Visser K, Nepveu M, Wassing BBT, Orlic B, Fokker PA (2014) Geomechanics response and induced seismicity during gas field depletion in the Netherlands. Geothermics 52:206–219

Wandycz P, Święch E, Eisner L et al (2019) (2019) Estimation of the quality factor based on the microseismicity recordings from Northern Poland. Acta Geophys 67:2005–2014. https://doi.org/10.1007/s11600-019-00362-7

Wcisło M, Stabile TA, Telesca L, Eisner L (2017) Variations of attenuation and VP/VS ratio in the vicinity of wastewater injection: a case study of Costa Molina 2 well (High Agri Valley, Italy). Geophysics 83:B25–B3.1

White RE (1992) The accuracy of estimating A from seismic data. Geophysics 57:1508–1511

Wessel P, Smith WHF (1991) Free software helps map and display data. EOS Trans AGU 72(441):445–446

Zang A, Volker Oye V, Jousset P, Deichmann N, Gritto R, McGarr A, Majer E, Bruhn D (2014) Analysis of induced seismicity in geothermal reservoirs—an overview. Geothermics. https://doi.org/10.1016/j.geothermics.2014.06.005

Zollo A, de Lorenzo S (2001) Source parameters and three-dimensional attenuation structure from the inversion of microearthquake pulse width data: method and synthetic tests. J Geophys Res 106:16-287–16-306